

Article

# Feedback Linearization-Based Control Strategy for Interlinking Inverters of Hybrid AC/DC Microgrids with Seamless Operation Mode Transition

Thanh Hai Nguyen <sup>1</sup>, Tan Luong Van <sup>2,\*</sup>, Asif Nawaz <sup>1</sup> and Ammar Natsheh <sup>1</sup>

<sup>1</sup> Faculty of Engineering Technology and Science, Higher Colleges of Technology, Dubai P.O. Box 16062, United Arab Emirates; nhai@hct.ac.ae (T.H.N.); anawaz@hct.ac.ae (A.N.); anatsheh@hct.ac.ae (A.N.)

<sup>2</sup> Department of Electrical and Electronics Engineering, Ho Chi Minh City University of Food Industry, 140 Le Trong Tan, Ho Chi Minh City 760310, Vietnam

\* Correspondence: luongvt@hufi.edu.vn; Tel.: +84-909653157

**Abstract:** This study proposes an advanced control scheme for the interlinking inverters of the hybrid AC/DC microgrids, which facilitates a seamless transition between grid-connected and stand-alone/islanding modes for the microgrid. Due to a nonlinear relationship between the terminal voltages of the voltage-source inverter (VSI) interfacing through inductor–capacitor (LC) filters with the grid voltages and currents, a feedback linearization technique (FLT) is employed to control the interlinking VSI under both grid-connected and islanding operations. The FLT-based current controllers are applied in the grid-connected mode, in which they adjust the power exchange between the DC and AC subgrids and mitigate the distortion of the grid currents produced by nonlinear loads. Under the stand-alone operation, the AC bus voltages are directly regulated by the FLT-voltage controllers of the interlinking VSI. In order to reduce the inrush currents and voltage overshoot at the instant of mode switching, the FLT-based controllers are performed all the time regardless of the operating modes, where the voltage references for the VSI are not changed abruptly. The control performance of the VSI is highly satisfactory with low-transient overshoot values of the voltages and currents and low total harmonic distortion (THD) values of the grid currents and AC bus voltages are about 3.5% and 2.7%, respectively, under the nonlinear load condition. The validity of the new control strategy is verified by the simulation work, which investigates the operation of a hybrid AC/DC microgrid.

**Keywords:** current controller; feedback linearization technique; hybrid AC/DC microgrid; seamless mode transition; voltage controller



**Citation:** Nguyen, T.H.; Van, T.L.; Nawaz, A.; Natsheh, A. Feedback Linearization-Based Control Strategy for Interlinking Inverters of Hybrid AC/DC Microgrids with Seamless Operation Mode Transition. *Energies* **2021**, *14*, 5613. <https://doi.org/10.3390/en14185613>

Academic Editor: Alberto Geri

Received: 7 August 2021

Accepted: 3 September 2021

Published: 7 September 2021

**Publisher's Note:** MDPI stays neutral with regard to jurisdictional claims in published maps and institutional affiliations.



**Copyright:** © 2021 by the authors. Licensee MDPI, Basel, Switzerland. This article is an open access article distributed under the terms and conditions of the Creative Commons Attribution (CC BY) license (<https://creativecommons.org/licenses/by/4.0/>).

## 1. Introduction

Today, with the requirement and utilization of both AC and DC electrical powers from the load and generation sides, a type of microgrid based on both DC and AC busbars called hybrid microgrid is an efficient solution, which has been paid remarkable attention in the past few years [1–6]. The hybrid microgrid contains both DC and AC common subgrids, which are interfaced through the interlinking voltage–source inverters [6,7]. Each subgrid is composed of renewable energy sources and loads, where the energy storage systems (ESSs) and the photovoltaic (PV) system are normally connected to the DC subgrid [8,9]. The amount of energy produced by the microgrid from the renewable energy systems is variable, which may cause an imbalance between the internal supply and demand of the microgrid. For this scenario, the microgrid is required to connect to the AC grid to transmit/receive the power to/from the AC grid, which ensures the power balance inside the microgrid. In cases of grid fault occurrence, the microgrid needs to be isolated from the faults by disconnecting it with the AC utility to prevent from damaging the

microgrid devices and components. Even with the disconnection from the AC grid, the microgrid should stay remained in operation to supply the power to highly critical loads such as medical equipment, the semiconductor industry, and broadcasting facilities from the internal generating sources. Generally, in order to comply with a high requirement of consumers and a highly reliable power system for the higher quality of the supplied power distribution, the microgrid is essentially required to be able to operate under off-grid and on-grid modes. Physically connecting or disconnecting the microgrid to the AC network is usually carried out through a semiconductor device-based static transfer switch (STS), which is simply controlled [10]. In terms of control and operation, the interlinking inverter of the microgrid is required to obtain fast, stable, and seamless transition modes between on-grid and off-grid operations, which deliver the powers to the grid under normal grid conditions and protect the microgrid and loads under the grid fault conditions [11–13].

The interlinking inverter is normally interfacing with the utility grid through inductor–capacitor (LC) filters, where the capacitor filter is essential for forming the AC voltages when the microgrid is operated under off-grid mode. In the grid-connected (GC) mode, the currents flowing between the microgrid and the grid through the interlinking inverter are adjusted to be sinusoidal, through which the real and reactive powers of the microgrid are controlled to supply to the local loads and the AC utility. Therefore, the interlinking inverter is working as a current-controlled VSI, where well-known proportional-integral (PI) controllers based on synchronous reference frame (SRF) have been widely employed to regulate the converter currents. This method is very simple and gives a satisfactory performance. Another control scheme based on the proportional-resonant (PR) regulators is employed for the control variables being AC signals, where the  $dq$ -axis components of converter currents will contain the AC components under the grid voltage distortion and/or the nonlinear loads [14,15]. When the microgrid is isolated from the utility under a grid fault such as voltage sag, swell, or interruption, the interlinking inverter plays a role to establish the AC load voltages at the nominal one for the operation of the AC loads [16,17]. This is the stand-alone (SA) operation mode of the hybrid microgrid. Similar to the current-controlled VSI, the PI regulators are employed for both the outer voltage control loop and inner current control loop [18,19]. The performance of the interlinking inverter employing the aforementioned linear control methods is normally deteriorated due to the nonlinear characteristic of the inverter. Furthermore, the cascaded control structure based on PI and PR requires considerable tuning, which is a time-consuming process to achieve a satisfactory control performance [20,21].

Another issue for the interlinking inverter of the microgrid is that the mode changing between the on-grid and off-grid operations may lead to the voltage surge across the critical loads or inrush current flowing to the grid. Few research studies have presented seamless transition between grid-connected and islanded operations to mitigate negative impacts from the current and voltage surges on the equipment and microgrid [19,22,23]. Authors in [19] have introduced a cascaded control scheme for the current and voltage, where a feedforward term is applied in the voltage controller. This provides a better response of the inverter when the operation mode changes. However, this method is basically a linear-based control method even with the feedforward voltage controller, which could not work well if nonlinear loads are connected to the microgrid. Another approach has been reported in [22], where the direct voltage controllers are employed for the interlinking inverter in both grid-connected and islanding modes. However, it has not been properly proved that the voltage controllers applying to the grid-tied inverter can be used to produce the current references or power delivered to the grid since that voltage is fixed and established by the grid. In addition, PI controllers are also employed in this method, which has the same shortcomings as that of the approach reported in [19] under the nonlinear load condition. Recently, the advanced control method based on model predictive control has been employed in the microgrid, which overcomes the drawbacks of the PI-resonant regulators [12]. However, the procedure and transient response of the inverter for the mode transition have not been taken into account properly.

In this research, an advanced control algorithm for the interlinking inverters of the hybrid AC/DC microgrids is proposed, where the feedback linearization technique is utilized to control the nonlinear-characterized voltage–source inverter. The interlinking inverter is allocated for the power exchange between the DC subgrid and the AC subgrids or the utility grid. Under the grid-connected operation, the inverter plays an essential role to maintain the DC-bus voltage, which leads to power balance exchanging among the DC subgrid, AC subgrid, and the main grid. Additionally, the interlinking inverter is utilized to provide an active filter operation mode, which eliminates the distorted currents generated from nonlinear loads before injecting them into the grid. For this mode, the FLT-based controllers for the phase currents of the inverter expressed in the SRF are applied. Meanwhile, under the off-grid mode, the AC bus voltages are established and maintained at the nominal one by the interlinking inverter only, where the FLT-voltage controllers are employed. In the off-grid operation mode, the DC-bus voltage is kept and regulated by the converter of the ESS, which assists in balancing the power between two subgrids. A seamless transition between on-grid and off-grid modes for the interlinking inverter is achieved through performing the FLT-based controllers continuously regardless of the operating modes by which the outputs of the controllers in deactivated mode are maintained closely with those in the activated mode. This prevents high inrush currents and voltage spikes while the operation mode of the interlinking inverter is changing. The PSIM simulation tests on the hybrid AC/DC microgrid with two-level VSI were carried out to verify the feasibility of the proposed algorithm.

## 2. System Description

An overall diagram of a hybrid microgrid containing the AC and DC subgrids is shown in Figure 1, where each subgrid consists of the generated power sources and its own loads. The AC subgrid may contain wind turbine systems, AC loads, and nonlinear loads, whose frequency is equal to the utility-rated frequency. The AC subgrid connects to the main grid through the point of common coupling (PCC). The PV system and the ESS are normally connected to the DC subgrid, which also contains the local DC loads.

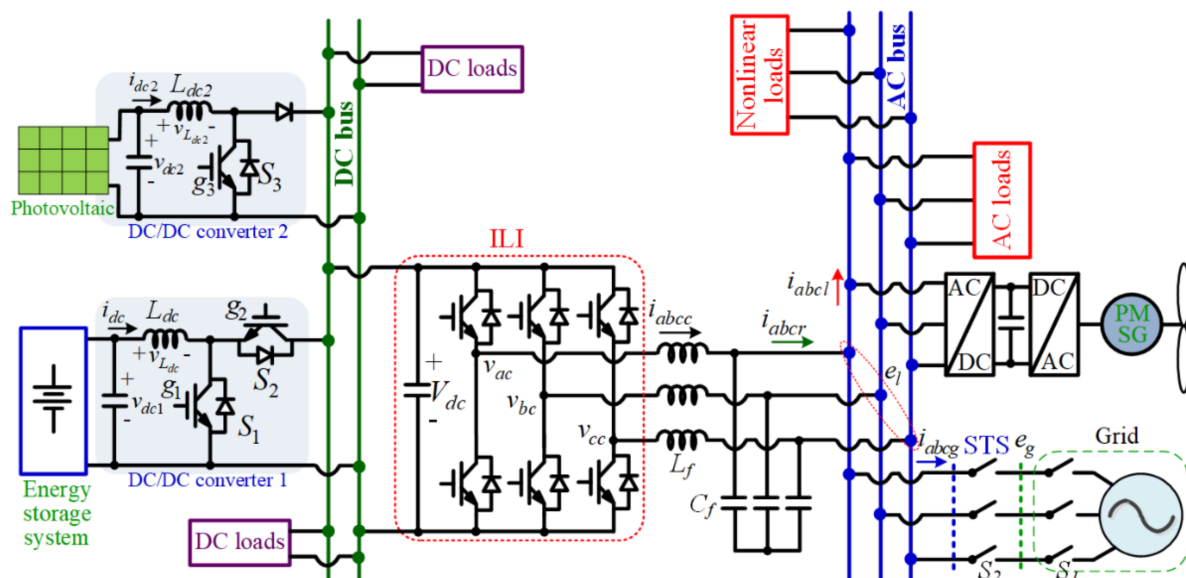


Figure 1. Schematic diagram of hybrid AC/DC microgrid.

The interlinking inverter (ILI) is a three-phase two-level voltage–source inverter, which assists to deliver the power between two subgrids as well as injects the power from the DC subgrid into the utility grid. The LC filters are used to interface the inverter with the AC subgrid, as shown in Figure 1. There are usually two STS switches,  $S_1$  and  $S_2$ , to perform connecting/disconnecting the microgrid to the utility grid, as seen in Figure 1. It is noted

in Figure 1 that the switch  $S_1$  is controlled by the main grid operator, while the microgrid monitors the AC voltage and line frequency, then using the  $S_2$  to isolate the microgrid if any fault occurs. Such fault conditions considered in this paper are voltage sag, swell, and line frequency variation out of allowable range. In general, the hybrid microgrid is able to operate in the on-grid and off-grid modes.

In the on-grid operation, the DC-link voltage is maintained by the ILI, which guarantees a power balance exchanged among the DC, AC subgrids, and the utility. In this mode, the PV and wind turbine renewable energy systems in the microgrid are operating in the maximum power point tracking (MPPT) control. Furthermore, the ILI can be working as an active filter to filter out the distorted currents caused by the nonlinear loads, which helps improve the THD of the grid currents. In the stand-alone mode, the ILI is allocated to form the AC-bus voltages at their nominal value, while the DC-bus voltage is controlled by the DC/DC converter of the ESS. If the capacity of the ESS is sufficient, the power balance between two subgrids will be obtained. Otherwise, some of the loads in the microgrid have to be shed.

### 3. Proposed Control Scheme of Hybrid Microgrid

FLT is a well-known control method, which has been applied in many different applications such as in power electronics and power systems [24,25]. The basic idea of feedback linearization is to transform a nonlinear system into a linear one by canceling its nonlinearities [26]. This work mainly focuses on the control of the single ILI under both on-grid and off-grid operation modes, which employs an advanced control method based on FLT. Therefore, the droop control to determine the power-sharing among the interlinking inverters in the microgrid is not considered in this paper. From Figure 1, the modeling of the ILI is expressed through  $dq$ -axis components of the voltages and currents as [27–29]

$$\dot{i}_{rd} = i_{cd} - C_f \dot{e}_{ld} + \omega_e C_f e_{lq} \quad (1)$$

$$\dot{i}_{rq} = i_{cq} - C_f \dot{e}_{lq} - \omega_e C_f e_{ld} \quad (2)$$

$$\dot{i}_{cd} = \frac{1}{L_f} v_{cd} - \frac{1}{L_f} e_{ld} + \omega_e i_{cq} \quad (3)$$

$$\dot{i}_{cq} = \frac{1}{L_f} v_{cq} - \frac{1}{L_f} e_{lq} - \omega_e i_{cd} \quad (4)$$

$$\dot{e}_{ld} = \frac{1}{C_f} i_{cd} - \frac{1}{C_f} i_{rd} + \omega_e e_{lq} \quad (5)$$

$$\dot{e}_{lq} = \frac{1}{C_f} i_{cq} - \frac{1}{C_f} i_{rq} - \omega_e e_{ld} \quad (6)$$

where  $i_{rdq}$  is the  $dq$ -axis components of the ILI output currents flowing into the AC bus,  $i_{cdq}$  is the  $dq$ -axis components of the ILI,  $e_{ldq}$  is the load voltages expressed in  $dq$  frame, which is the same as the grid voltages,  $e_{gdq}$ , in the grid-connected mode, and  $v_{cdq}$  is the  $dq$ -axis inverter terminal voltages.  $L_f$  and  $C_f$  are the filter inductance and capacitance, respectively, and  $\omega_e$  is the fundamental angular frequency of the utility grid.

#### 3.1. Control of the ILI in Grid-Tied Mode

As mentioned previously, the ILI is allocated to regulate the DC-bus voltage and deliver the active/reactive powers among DC, AC subgrids, and the grid by controlling the inverter currents. FLT is employed for the inverter current controllers, which is derived as follows:

By differentiating the inverter output currents once and substituting Equations (3) and (4) into Equations (1) and (2), one can obtain

$$\dot{i}_{rd} = \dot{i}_{cd} - C_f \ddot{e}_{ld} + \omega_e C_f \dot{e}_{lq} = -C_f \ddot{e}_{ld} + \omega_e C_f \dot{e}_{lq} - \frac{1}{L_f} e_{ld} + \omega_e i_{cq} + \frac{1}{L_f} v_{cd} \quad (7)$$

$$\dot{i}_{rq} = \dot{i}_{cq} - C_f \ddot{e}_{lq} - \omega_e C_f \dot{e}_{ld} = -C_f \ddot{e}_{lq} - \omega_e C_f \dot{e}_{ld} - \frac{1}{L_f} e_{lq} - \omega_e i_{cd} + \frac{1}{L_f} v_{cq} \quad (8)$$

From Equations (7) and (8), the ILI can be expressed through the state equations as [27]

$$\begin{aligned} \dot{\mathbf{x}} &= \mathbf{f}(\mathbf{x}) + \mathbf{B}\mathbf{u} \\ \mathbf{y} &= \mathbf{C}\mathbf{x} \end{aligned} \quad (9)$$

where  $\mathbf{x}$  is the state variables,  $\mathbf{u}$  is the inputs, and  $\mathbf{y}$  is the outputs, which are chosen as

$$\begin{aligned} \mathbf{x} &= [x_1 x_2 x_3 x_4]^T = [i_{rd} i_{rq} i_{cd} i_{cq}]^T, \\ \mathbf{u} &= [u_1 u_2]^T = [v_{cd} v_{cq}]^T, \mathbf{y} = [y_1 y_2]^T = [i_{rd} i_{rq}]^T \end{aligned} \quad (10)$$

and

$$\mathbf{f}(\mathbf{x}) = \begin{bmatrix} f_1(\mathbf{x}) \\ f_2(\mathbf{x}) \end{bmatrix} = \begin{bmatrix} -C_f \ddot{e}_{ld} + \omega_e C_f \dot{e}_{lq} - \frac{1}{L_f} e_{ld} + \omega_e x_4 \\ -C_f \ddot{e}_{lq} - \omega_e C_f \dot{e}_{ld} - \frac{1}{L_f} e_{lq} - \omega_e x_3 \\ -\frac{1}{L_f} e_{ld} + \omega_e x_4 \\ -\frac{1}{L_f} e_{lq} - \omega_e x_3 \end{bmatrix}$$

$$\mathbf{B} = \begin{bmatrix} B_1 \\ B_2 \end{bmatrix} = \begin{bmatrix} \frac{1}{L_f} & 0 \\ 0 & \frac{1}{L_f} \\ \frac{1}{L_f} & 0 \\ 0 & \frac{1}{L_f} \end{bmatrix}, \mathbf{C} = \begin{bmatrix} 1 & 0 & 0 & 0 \\ 0 & 1 & 0 & 0 \end{bmatrix}$$

It can be rewritten from Equations (9) and (10) as

$$\dot{\mathbf{y}} = \mathbf{f}_1(\mathbf{x}) + \mathbf{B}_1 \mathbf{u} \quad (11)$$

The nonlinear terms between the inputs and outputs of the ILI modelling can be decoupled by defining another variable matrix, which is new control inputs,  $\mathbf{v}$ , expressed as follows:

$$\mathbf{u} = \mathbf{B}_1^{-1}(-\mathbf{f}_1(\mathbf{x}) + \mathbf{v}) \quad (12)$$

The new control inputs can be expressed in the Laplace domain by adding the tracking controllers as

$$\begin{bmatrix} v_1 \\ v_2 \end{bmatrix} = \begin{bmatrix} s y_1^* - k_{11} e_1 - k_{12} \frac{1}{s} e_1 - k_{13} \frac{s}{s^2 + (6\omega_e)^2} e_1 \\ s y_2^* - k_{21} e_2 - k_{22} \frac{1}{s} e_2 - k_{23} \frac{s}{s^2 + (6\omega_e)^2} e_2 \end{bmatrix} \quad (13)$$

where  $e_1 = i_{rd} - i_{rd}^*$ ,  $e_2 = i_{rq} - i_{rq}^*$ , and  $k_{ij}$  ( $i = 1 \sim 2$ ,  $j = 1 \sim 3$ ) are the gains of tracking controllers, and  $y_i^*$  ( $i = 1 \sim 2$ ) refer to the controlled variables, which are  $i_{rd}^*$  and  $i_{rq}^*$ . It is noted that the fifth- and seventh-order harmonic components of the load currents and voltages in a three-phase frame appear due to the nonlinear loads of the microgrid. Then, through transforming the three-phase variables to two-phase variables expressed in the SRF, the  $dq$ -axis components of the currents and voltages contain DC and the sixth-order components. Therefore, the tracking controllers consist of the integral and resonant regulators, which are used to suppress the errors in steady-state for the state variables being in both the DC and AC signals, as shown in (13).

### 3.2. Control of the ILI in Stand-Alone Mode

In the islanding mode, the AC-bus voltages are formed by the ILI and are directly controlled by FLT. Similar to the previous subsection, the FLT-based voltage controllers of the ILI are developed as follows: From Equations (5) and (6), the load voltages expressed in the  $dq$ -axis components can be rewritten by differentiating twice as

$$\begin{aligned}\ddot{e}_{ld} &= \frac{1}{C_f} \dot{i}_{cd} - \frac{1}{C_f} \dot{i}_{rd} + \omega_e \dot{e}_{lq} \\ &= \frac{2\omega_e}{C_f} i_{cq} - \frac{1}{C_f} \dot{i}_{rd} - \frac{\omega_e}{C_f} i_{rq} - \left(\frac{1}{C_f L_f} + \omega_e^2\right) e_{ld} + \frac{1}{C_f L_f} v_{cd}\end{aligned}\quad (14)$$

$$\begin{aligned}\ddot{e}_{gq} &= \frac{1}{C_f} \dot{i}_{cq} - \frac{1}{C_f} \dot{i}_{rq} - \omega_e \dot{e}_{ld} \\ &= -\frac{2\omega_e}{C_f} i_{cd} - \frac{1}{C_f} \dot{i}_{rq} + \frac{\omega_e}{C_f} i_{rd} - \left(\frac{1}{C_f L_f} + \omega_e^2\right) e_{lq} + \frac{1}{C_f L_f} v_{cq}\end{aligned}\quad (15)$$

The state equations of the ILI for controlling the AC-bus voltages are expressed in the form as

$$\begin{aligned}\dot{\mathbf{x}} &= \begin{bmatrix} x_3 \\ x_4 \\ f_3(\mathbf{x}) \end{bmatrix} + \begin{bmatrix} 0_{2 \times 2} \\ D \end{bmatrix} \mathbf{u} \\ \mathbf{y} &= E\mathbf{x}\end{aligned}\quad (16)$$

where the state variables, inputs, and outputs for the FLT-based voltage controllers are chosen as

$$\begin{aligned}\mathbf{x} &= [x_1 x_2 x_3 x_4]^T = [e_{ld} e_{lq} \dot{e}_{ld} \dot{e}_{lq}]^T, \\ \mathbf{u} &= [u_1 u_2]^T = [v_{cd} v_{cq}]^T, \\ \mathbf{y} &= [y_1 y_2]^T = [e_{ld} e_{lq}]^T\end{aligned}\quad (17)$$

and

$$\begin{aligned}f_3(\mathbf{x}) &= \begin{bmatrix} \frac{2\omega_e}{C_f} i_{cq} - \frac{1}{C_f} \dot{i}_{rd} - \frac{\omega_e}{C_f} i_{rq} - \left(\frac{1}{C_f L_f} + \omega_e^2\right) x_1 \\ -\frac{2\omega_e}{C_f} i_{cd} - \frac{1}{C_f} \dot{i}_{rq} + \frac{\omega_e}{C_f} i_{rd} - \left(\frac{1}{C_f L_f} + \omega_e^2\right) x_2 \end{bmatrix} \\ D &= \begin{bmatrix} \frac{1}{C_f L_f} & 0 \\ 0 & \frac{1}{C_f L_f} \end{bmatrix}, E = [I_{2 \times 2} \quad 0_{2 \times 2}]\end{aligned}$$

From Equations (15) and (16), the nonlinear relationship of the outputs and inputs can be expressed as

$$\ddot{\mathbf{y}} = f_3(\mathbf{x}) + D\mathbf{u}\quad (18)$$

Then, the new inputs are defined to decoupling the nonlinear term and are expressed as

$$\mathbf{u} = D^{-1}(-f_3(\mathbf{x}) + \mathbf{v})\quad (19)$$

and

$$\begin{bmatrix} v_1 \\ v_2 \end{bmatrix} = \begin{bmatrix} s^2 y_1^* - k_{31} s e_1 - k_{32} e_1 - k_{33} \frac{1}{s} e_1 \\ s^2 y_2^* - k_{41} s e_2 - k_{42} e_2 - k_{43} \frac{1}{s} e_2 \end{bmatrix}\quad (20)$$

where  $e_1 = e_{ld} - e_{ld}^*$ ,  $e_2 = e_{lq} - e_{lq}^*$ ,  $k_{ij}$  ( $i = 3 \sim 4, j = 1 \sim 3$ ) are the gains of tracking controllers for the control variables  $y_i^*$  ( $i = 1 \sim 2$ ), which are  $e_{ld}^*$  and  $e_{lq}^*$ . In this operation mode, the  $e_{ld}$  is regulated to zero, and  $e_{lq}$  is maintained at the nominal amplitude of the grid voltage being constant. Therefore, the new control inputs contain the tracking controllers with an integral part only to eliminate the steady-state error.

It is worth noting that the gains of tracking controllers for both the FBT-based current and voltage controllers can be easily obtained through the pole-placement technique, where the desired poles are located on the left-half plane to obtain the closed-loop control stability [26,29].

### 3.3. Control of the DC/DC Converters for the ESS and PV

As mentioned above, the PV is operated in the MPPT control regardless of the operating modes of the microgrid, while the ESS operation depends on the microgrid status. When the microgrid is operating in the grid-tied mode, the ESS can be floating or charging/discharging the power from/to the microgrid depending on the battery state-of-charge (SOC) and powers generated from the PV and load demand. Inversely, in the stand-alone mode of the microgrid, the ESS is allocated to regulate the DC-link voltage, which is assumed that the ESS is capable of balancing the power between the demand and supply in the microgrid.

For the control targets of the aforementioned ESS and PV, the cascaded control of voltage and current is generally employed for the DC/DC choppers of the ESS and PV, which can be slightly modified to accomplish the requirements of the microgrid [30]. The DC voltage outer control loop is outputting the current reference for the filter inductor,  $i_{dc}^*$ , where the PI regulators are applied as

$$i_{dc}^* = (k_{51} + \frac{k_{52}}{s})(V_{dc}^* - V_{dc}) \quad (21)$$

where  $V_{dc}$  and  $V_{dc}^*$  are the voltage and its reference in the DC subgrid, respectively.  $k_{51}$  and  $k_{52}$  are the PI controller gains, respectively.

The inner controller regulates the current of the filter inductor, where its output is the voltage reference drop on the inductor,  $v_{L_{dc}}^*$ , expressed as

$$v_{L_{dc}}^* = (k_{61} + \frac{k_{62}}{s})(i_{dc}^* - i_{dc}) \quad (22)$$

where  $i_{dc}$  is the filter inductor current,  $k_{61}$  and  $k_{62}$  are the PI controller gains, respectively.

Then, the duty cycle of the DC/DC converter,  $d_{dc}$ , is calculated as

$$d_{dc} = \frac{v_{dci} + v_{L_{dc}}^*}{V_{dc}} \quad (23)$$

where  $v_{dci}$  is the DC input voltage of the ESS or PV array.

A control block diagram of the ILI and the DC/DC converter for both the operation modes of the microgrid is shown in Figure 2, which is explained in detail with the transition mode scheme in the next section.

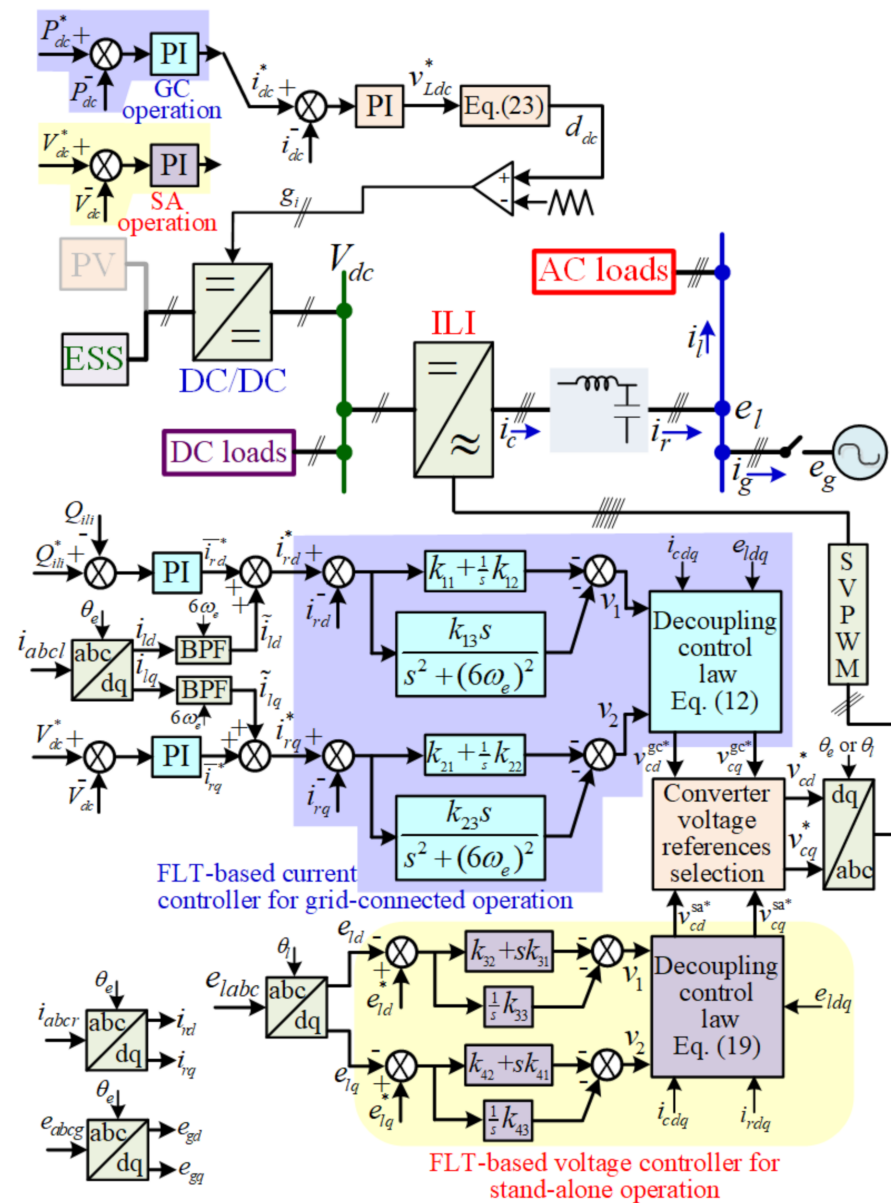


Figure 2. Control block diagram of the ILI and DC/DC converter in microgrid under both operation modes.

#### 4. Proposed Seamless Transition Scheme for Hybrid Microgrid

Figure 2 shows the detailed control block diagram for the ILI and DC/DC converters in the microgrid under both on-grid and off-grid operations, where the controllers are introduced in the previous section.

##### 4.1. Grid-Connected Operation Mode

Under the grid-tied operation, the ILI is employed to maintain the common voltage of the DC subgrid, regulate the reactive power to the grid and compensate the distorted currents from the nonlinear loads. The current references of the  $dq$ -axis components for the FLT-current controllers are obtained as

$$i_{rd}^* = \bar{i}_{rd}^* + \tilde{i}_{ld} \quad \text{and} \quad i_{rq}^* = \bar{i}_{rq}^* + \tilde{i}_{lq} \quad (24)$$

where  $\bar{i}_{rd}^*$  and  $\bar{i}_{rq}^*$  are  $dq$ -axis current component references being the outputs of reactive power and DC-bus voltage controllers, respectively.  $\tilde{i}_{ld}$  and  $\tilde{i}_{lq}$  are the AC components of

$dq$ -axis load currents, which are obtained through band-pass filters (BPFs). The three-phase nonlinear loads are considered, which produce fifth- and seventh-order harmonics in abc frame and become sixth-order harmonic in the  $dq$ -frame. Then, FLT-based current controllers are performed to regulate the ILI output currents including the linear and nonlinear terms, which produce the inverter terminal voltage references as  $v_{cd}^{gc*}$  and  $v_{cq}^{gc*}$ , respectively.

Under this operation mode, the DC/DC converters of the PV system and the ESS control their powers,  $P_{dc}^*$ , determined by the MPPT or demand from the microgrid, respectively, which generates the current references of the filter inductor,  $i_{dc}^*$ , for the inner current control loop, as seen in the top diagram in Figure 2.

#### 4.2. Stand-Alone Operation Mode

The common voltage of the DC subgrid is controlled by the DC/DC converter of the ESS under the islanding operation mode, where the control block diagram is shown in the top diagram in Figure 2. The detailed controllers are derived in Section 3.3. This controller action helps in balancing the power between the AC and DC subgrids and provides a stable input DC voltage for the ILI to work as a voltage source to control the AC-bus voltage. FLT-based controllers are employed to control the AC-bus voltages directly, where the references for the  $dq$ -axis components,  $e_{ldq}^*$ , are set as

$$e_{ld}^* = 0 \quad \text{and} \quad e_{lq}^* = E_g \quad (25)$$

where  $E_g$  is the nominal magnitude of the grid voltage. The outputs of FLT-based voltage controllers are the  $dq$ -axis components of the inverter terminal voltage references,  $v_{cd}^{sa*}$  and  $v_{cq}^{sa*}$ , which are illustrated in the bottom diagram in Figure 2.

#### 4.3. Transition from Grid-Tied to Islanding Modes

The grid is considered faulty when its voltage amplitude is lower than 90% (voltage sag) or higher than 110% (voltage swell), compared to the rating, or the grid-frequency variation is higher than 1% with respect to the fundamental frequency. In this work, the grid voltage expressed through  $e_{gd}$  and  $e_{gq}$  was monitored and compared to the nominal values, where the grid voltage vector is aligned with the  $q$ -axis. Therefore,  $e_{gd}$  is mostly zero, and  $e_{gq}$  is the magnitude of the grid voltage.

When a grid fault condition is detected, the DC/DC chopper of the ESS is immediately switching to control the DC-bus voltage, while the grid currents are controlled to be reduced intentionally close to zero by the ILI. For achieving this, the current references for the FLT-based current controller of the ILI are set as

$$i_{rd}^* = i_{ld} \quad \text{and} \quad i_{rq}^* = i_{lq} \quad (26)$$

where  $i_{ld}$  and  $i_{lq}$  are the load currents of  $dq$ -axis components, respectively. When the grid currents approach zero, the STS is switched off to isolate the microgrid from the fault. Then, the stand-alone mode is activated and FLT-based voltage controllers are performed to regulate the AC-bus voltages following its reference, as in Equation (25). In order to achieve a seamless transition, the load voltage phase angle is set to be continuous with the grid voltage phase angle at the mode switching moment. In addition, the frequency of the AC-bus voltages is set the same as that of the grid. Therefore, the phase angle of the load AC voltage,  $\theta_l$ , is expressed as

$$\theta_l = \int \omega_e dt + \theta_{l0} \quad (27)$$

where  $\theta_{l0} = \theta_e$  is the initial phase angle of the load AC voltage, and  $\theta_e$  is the phase angle of the grid voltage at the mode transition moment.

The output voltage references of the inverter,  $v_{cd}^*$  and  $v_{cq}^*$ , are selected as the outputs of the FLT-based voltage controllers expressed as

$$v_{cd}^* = v_{cd}^{sa*} \quad \text{and} \quad v_{cq}^* = v_{cq}^{sa*} \quad (28)$$

Even though the outputs of FLT-based current controllers are not used in the stand-alone mode, FLT-based current controllers continue running with the current references as in Equation (26) to generate the controller outputs,  $v_{cd}^{gc*}$  and  $v_{cq}^{gc*}$ , being close to the effective voltage references of the inverter. This helps the voltage references not to change abruptly, and the smooth transition can be easily obtained.

#### 4.4. Transition from Islanding to Grid-Connected Modes

Even when the microgrid is operated under islanding mode, the microgrid still monitors the grid AC voltage. When the grid voltages are recovered from the sag/swell, then the microgrid is reconnected to the main grid for the on-grid operation mode. Prior to closing the STS for the grid-connected operation, the synchronization of the voltages of the AC subgrid with the main grid voltages in terms of phase, frequency, and amplitude is required to avoid causing the current spikes. If the differences of the phase angle and amplitude of the two voltages are higher than the thresholds, selected as 0.01 pu in this work, the ILI is still operated under voltage-controlled mode to regulate the AC-bus voltages matching with the grid voltages in terms of the phase and magnitude. It is noted that if the phase angles of the two voltages are fully matched, the frequencies of the voltages are naturally the same. When the phase and amplitude of the grid and AC-bus voltages are matched, the switches STS are closed and the microgrid starts operating in grid-tied mode. At this instant, the DC/DC chopper of the ESS is switching to the power control, and the ILI performs FLT-current controllers to adjust the DC-bus voltage, reactive power, and harmonic current compensation, where the current references are determined, as in Equation (24).

It is worth noting that before switching to grid-connected mode, FLT-based current controllers are still running. Therefore, when the operation mode is switched with the current reference change, the ILI responds to the variation of the references. This helps reduce the transient overshoot values of the currents and voltages at the mode transition. In this operation mode, the outputs of the FLT-based current controllers are used for the inverter voltage references to be modulated as

$$v_{cd}^* = v_{cd}^{gc*} \quad \text{and} \quad v_{cq}^* = v_{cq}^{gc*} \quad (29)$$

In addition, for obtaining the smooth transition from the grid-tied mode to the islanding mode, FLT-based voltage controllers are still performed during the grid-tied mode, where the voltage references are selected as

$$e_{ld}^* = e_{gd} \quad \text{and} \quad e_{lq}^* = e_{gq} \quad (30)$$

## 5. Results and Discussion

In order to prove the effectiveness of the suggested control method, simulation tests for a 15-kW microgrid presented in Figure 1 by PSIM software were performed. The DC-bus voltage is maintained at 400 V. A three-phase two-level VSI was utilized for the ILI between the AC and DC subgrids. The PV array and the ESS are represented by a constant DC voltage source of 200 V integrating into the DC subgrid through a DC/DC converter. In the AC subgrid, the local loads contain a three-phase RL load of  $12 + j9.4(\Omega)$  and a DC resistor load of 10  $\Omega$  connecting at the DC side of a three-phase diode rectifier. The STS is represented by the bidirectional switches, which were utilized to connect/disconnect the microgrid to/from the grid. The parameters of the studied microgrid are listed in Table 1. The gains of the controllers introduced in Figure 2 were determined according to the design

criteria of the pole-placement technique, which were then tuned further by a trial-and-error method [26,30]. These gains are listed in Table 2.

**Table 1.** Parameters of hybrid microgrid.

Components	Parameters	Values
ILI	Power rating	15 kW
	Grid voltage	180 V/60 Hz
	LC filters	3 mH/50 $\mu$ F
	DC-link capacitor	3.3 mF
	Sampling frequency	10 kHz
	Switching frequency	5 kHz
DC/DC converter	DC inductance	3 mH
	DC-bus voltage	400 V
	Switching frequency	2.5 kHz

**Table 2.** Controller gains.

Converters	Controllers	Gains
ILI	FLT-current controllers	$k_{11} = k_{21} = 17.5 \times 10^3$ $k_{12} = k_{22} = 2.1 \times 10^6$ $k_{13} = k_{23} = 0.836 \times 10^9$
	FLT-voltage controllers	$k_{31} = k_{41} = 6.25 \times 10^3$ $k_{32} = k_{42} = 2.75 \times 10^6$ $k_{33} = k_{43} = 0.215 \times 10^9$
	DC-voltage controller	$K_P = 0.71$ ; $K_I = 142$
DC/DC converter	Voltage regulator	$K_P = 0.375$ ; $K_I = 18.5$
	Current regulator	$K_P = 1.5$ ; $K_I = 1500$

Figure 3 illustrates the control performance of the microgrid, where the microgrid is operated in the grid-tied mode and islanding mode, as well as in the transient conditions such as mode transition and the load changes in the subgrids in both the AC and DC sides. The investigated operation conditions are as follows:

- A grid voltage sag occurs from 1.2 s to 1.8 s. The microgrid is operated in the islanding mode within this duration;
- ESS power is changed at 0.75 s from 12 kW to 60 kW during the grid-connected mode. An additional RL load of  $12 + j5.7(\Omega)$  is added to the AC subgrid during the stand-alone operation.

Waveforms of three-phase currents of the loads, the ILI output, and the grid are shown in Figure 3a–c, respectively, and Figure 3d shows the  $dq$ -axis components of the ILI currents, which are magnified in Figures 4 and 5. It is seen in Figure 3c that no current flows into the grid during the stand-alone mode from 1.2 s to 1.8 s, where the currents of the load in the AC subgrid are the same as those of the ILI output, as seen in Figure 3a,b. Figure 3e shows the  $dq$ -axis components of the grid and AC-bus voltages, which demonstrates that the AC-bus voltages are well maintained at the nominal value of 180 V when a grid sag occurs. Figure 3f shows the outputs of FLT-based controllers for the current and voltage. It is seen in Figure 3g that the DC-bus voltage is well kept at 400 V under both the GC and SA modes and the transient conditions of the load changes. Figure 3h shows the DC-inductor currents of the DC/DC converter, which shows the highly satisfactory performance of the DC-inductor current controller.

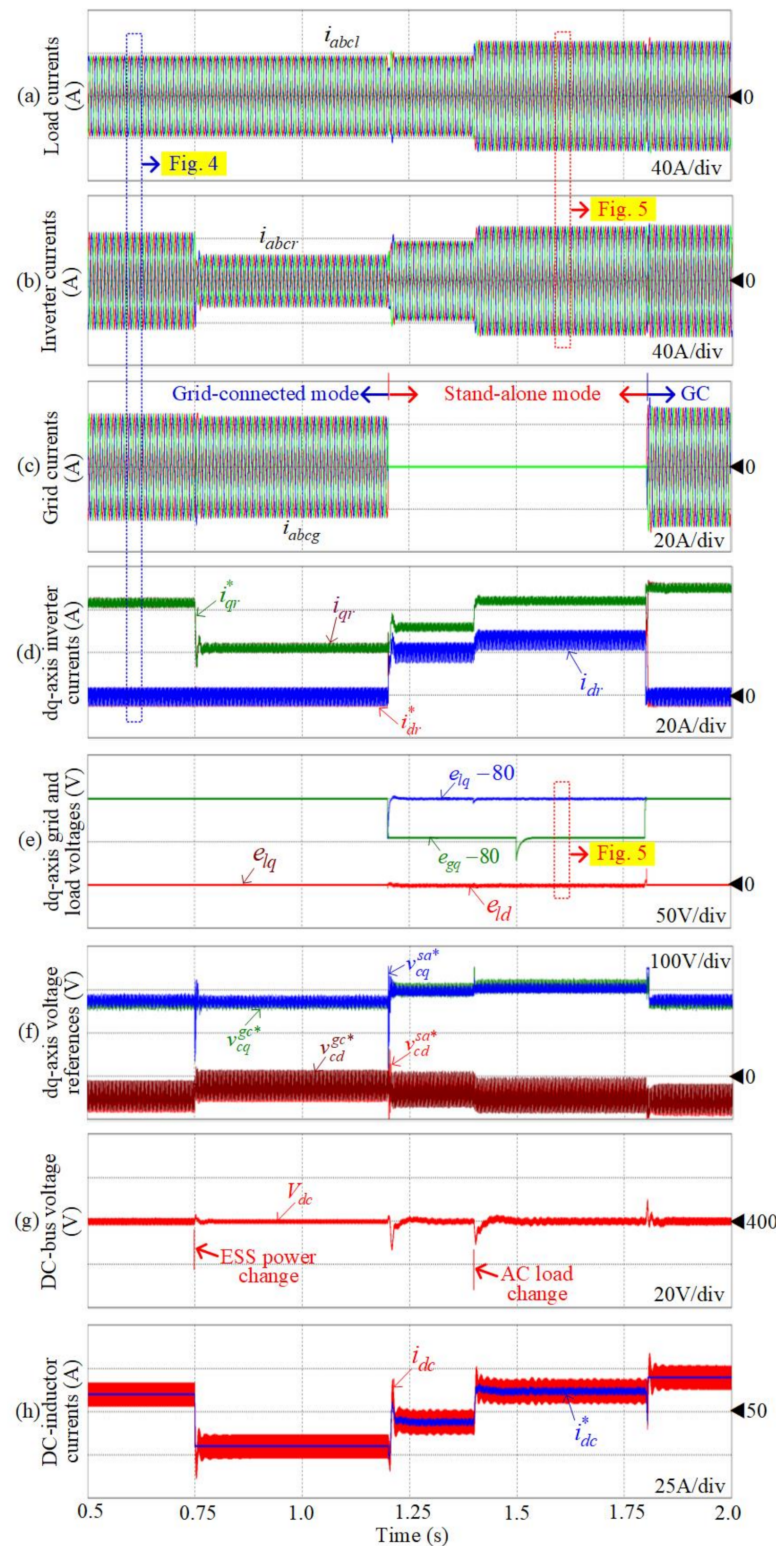


**Figure 3.** Control performance of the microgrid under both the grid-tied and stand-alone modes and transition: (a) load currents; (b) inverter output currents; (c) grid currents; (d)  $dq$ -axis components of inverter currents; (e)  $dq$ -axis components of the grid and load voltages; (f) voltage references for both modes; (g) DC-bus voltage; (h) DC-inductor currents.

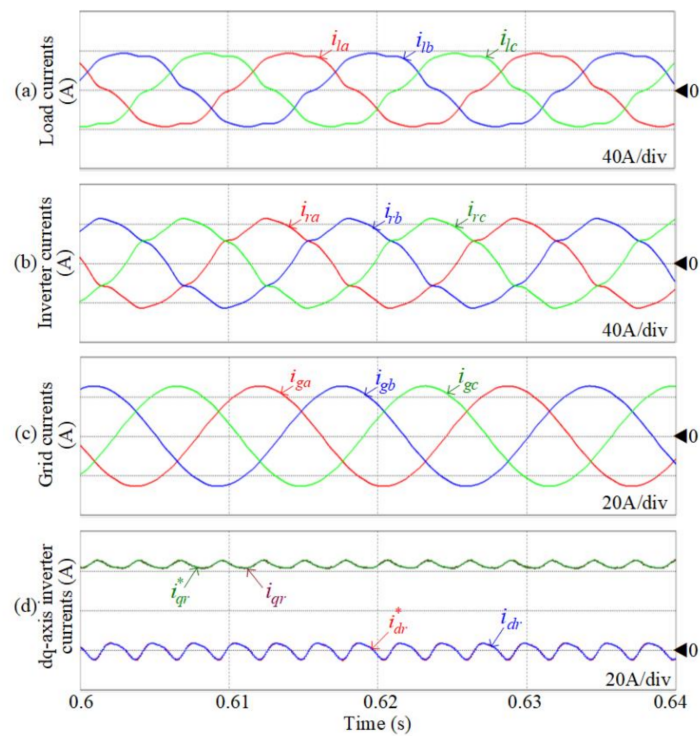


**Figure 4.** Control performance of the microgrid under the grid-connected modes: (a) load currents; (b) inverter output currents; (c) grid currents; (d)  $dq$ -axis components of inverter currents.

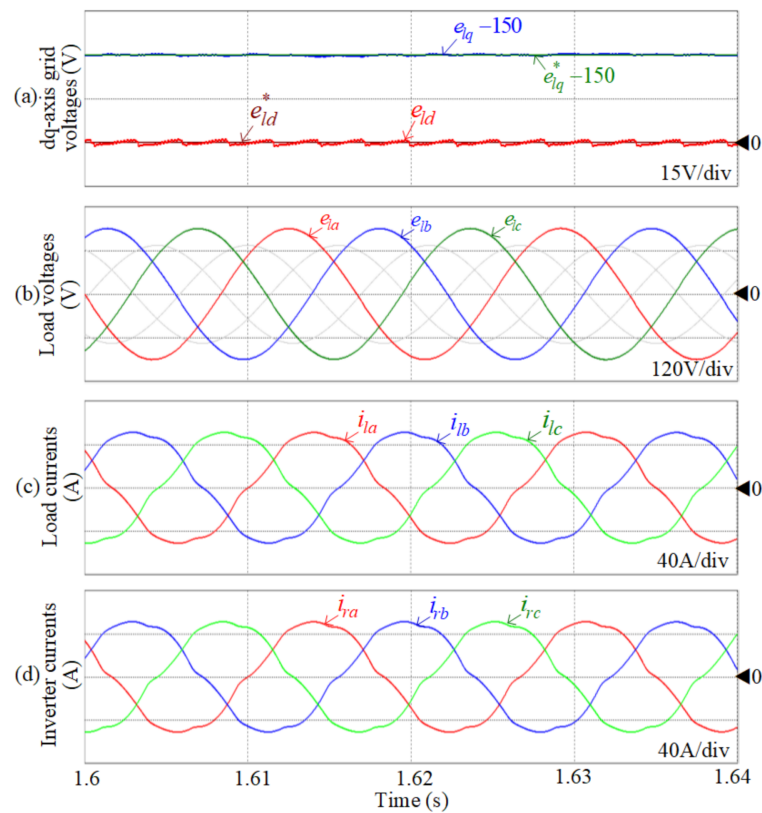


**Figure 5.** Control performance of the microgrid under the stand-alone modes: (a)  $dq$ -axis components of the load voltages; (b) load phase voltages; (c) load currents; (d) inverter output currents.

Figure 4 magnifies the waveforms of the currents presented in Figure 3. Due to the presence of the nonlinear load, the phase currents of the load are distorted, as shown in Figure 4a, where its THD is about 8.2%. By compensating the current distortion from the ILT, where the inverter currents are also distorted, as shown in Figure 4b, the grid phase currents are improved and become more sinusoidal with a low THD value of about 3.5%. The  $dq$ -axis components of the inverter currents are shown in Figure 4d, which shows that the actual currents track their references closely. This demonstrates that FLT-based current controllers work well.

The performance of the FLT-based voltage controllers for the microgrid operating in the stand-alone mode is illustrated in Figure 5. Figure 5a shows the  $dq$ -axis components of the AC-bus voltage when the grid voltages drop to 0.75 pu. It is seen that the  $q$ -axis component of the AC-bus voltage is controlled well at 180 V, and the  $d$ -axis component is regulated at 0. Figure 5b shows the three-phase AC-bus voltages, which are well balanced and sinusoidal with a low THD value of 2.7%. These results indicate that the proposed control scheme gives a better performance, compared to the conventional method, which is the traditional PI controller with the load current feedforward report in [15]. For this method, the THD of the load voltages is 3.2%. By maintaining the AC-bus voltages, the loads in the AC subgrid are continuously supplied. Figure 5c shows the load three-phase currents, which are the same as those of the inverter, as shown in Figure 5d.

The response of the mode transition from the GC to SA operation is demonstrated in Figure 6. To achieve a smooth transition, the FLT-based voltage controllers are still performed, as presented in Section 4.3. Therefore, it is seen in Figure 6a that the outputs of the FLT-based voltage controllers and the FLT-based current controllers expressed in the  $dq$  frame are similar during the grid-connected operation before the fault occurrence at 1.2 s. Figure 6b shows the three-phase AC-bus voltages, which are the same as the grid voltages and smoothly regulate the nominal value when the STS is open. When the mode transition is occurring, the initial phase angle of the AC-bus voltage is set as the phase angle of the grid voltage, which is shown in Figure 6c.

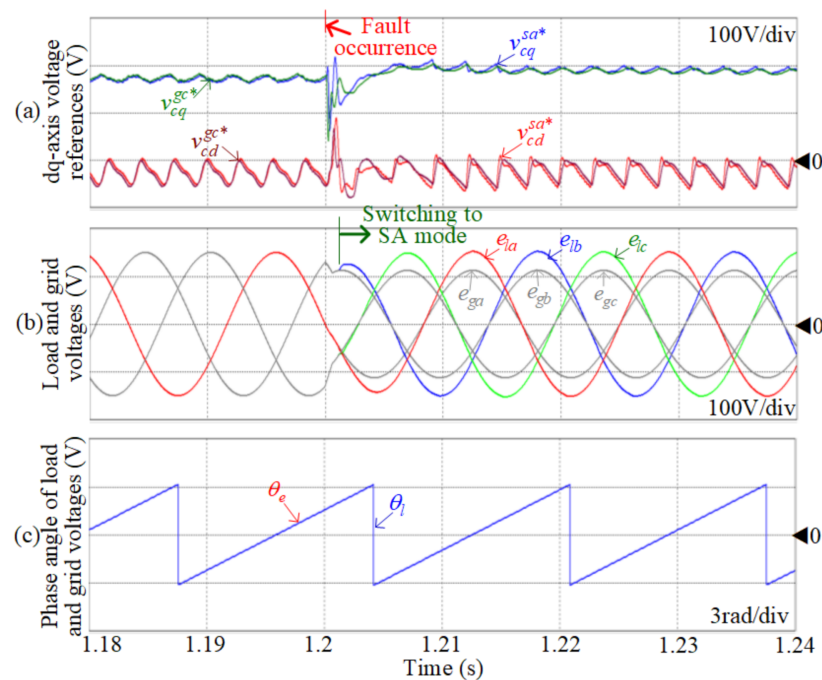


**Figure 6.** Transition performance from GC operation to SA operation: (a)  $dq$ -axis voltage references; (b) load and grid phase voltages; (c) phase angles.

Figure 7 shows the performance of the microgrid while switching from the SA mode to the GC operation. It is seen in Figure 7a that during the SA operation before 1.8 s,

the outputs of FLT-based current controllers are similar to those of the FLT-based voltage controllers. When the grid fault is recovered, the AC-bus voltages are adjusted to follow the grid voltages in terms of magnitude and phase angle. After about 13 ms from the fault clearance, the microgrid is smoothly switching to the GC mode, where the phase voltages and its phase angle are well in agreement with those of the grid voltages without a transient, as shown in Figure 7b,c, respectively.

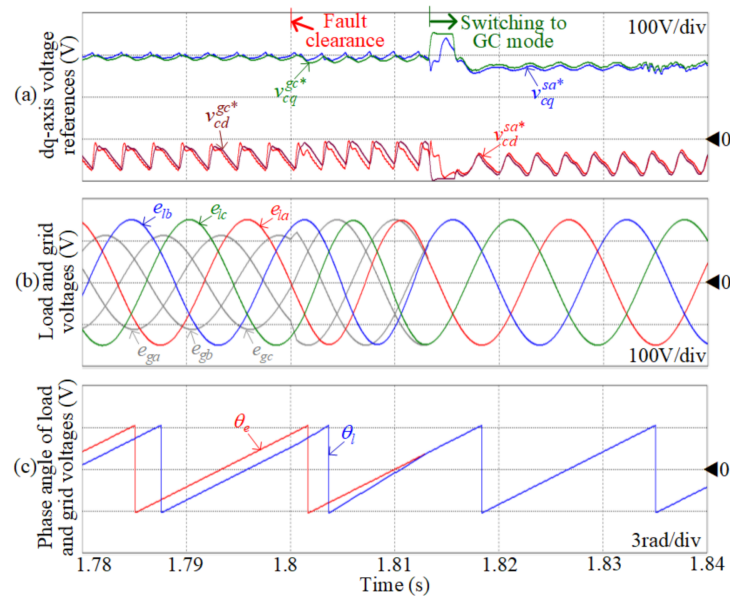


**Figure 7.** Transition performance from SA operation to GC operation: (a)  $dq$ -axis voltage references; (b) load and grid phase voltages; (c) phase angles.

Figure 8 shows the performance of the interlinking inverter under the condition of parameter variation for the islanding mode, where the filter inductance value,  $L_f$ , is changed from 3 mH to 2 mH at 1.6 s. Figure 8a shows the  $dq$ -axis load voltages, which are well regulated before and after the inductance change. At the moment of the inductance change, the overshoot of the  $dq$ -axis voltage components occurs, which is low and less than 1%, compared to the nominal voltage. Therefore, the three-phase voltages of the load are not affected, which are sinusoidal and balanced, as shown in Figure 8b.

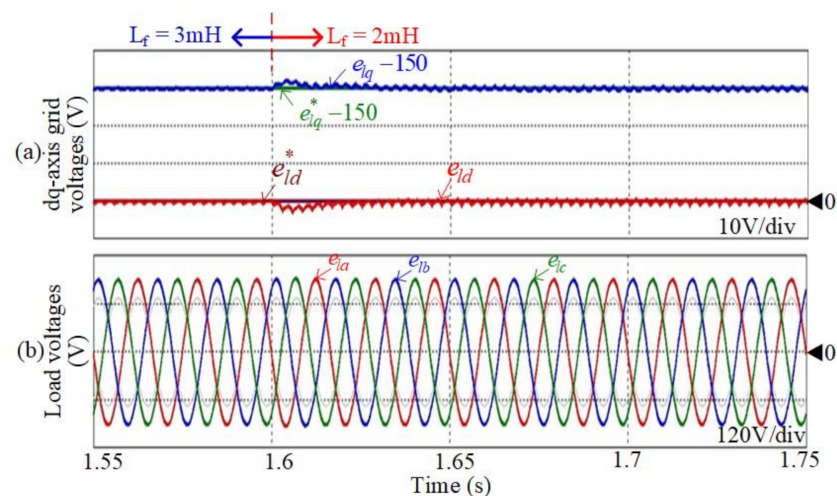


**Figure 8.** Control performance of the interlinking inverter under parameter variation: (a)  $dq$ -axis components of the load voltages; (b) load phase voltages.

## 6. Conclusions

This study proposed an advanced control algorithm for the interlinking inverters of the hybrid AC/DC microgrids, which utilizes the feedback linearization technique to deal with the nonlinear characteristics of the inverter. In addition, a seamless transition between grid-tied and islanding modes for the microgrid was also obtained by performing FLT-based current and voltage controllers of the ILI continuously regardless of the operation modes. In the steady-state condition, the FLT-based controllers work well to regulate the grid currents in the on-grid mode or maintain the AC-bus voltages in the off-grid mode under the nonlinear load and load change conditions. Furthermore, a procedure of control switching between the current controllers in the on-grid mode and the voltage controllers in the off-grid mode was presented in detail. The effectiveness of the suggested control scheme is proven by the simulation results for a hybrid AC/DC microgrid, which demonstrate that the THD values of the grid currents and AC-bus voltages under 8.2% THD-distorted load current condition are 3.5% and 2.7% for the grid-tied and islanding operations, respectively.

**Author Contributions:** Conceptualization, T.H.N.; methodology, T.H.N.; software, T.H.N., T.L.V., A.N. (Asif Nawaz) and A.N. (Ammar Natsheh); validation, T.H.N.; formal analysis, T.H.N.; investigation, T.H.N.; resources, T.H.N., T.L.V., A.N. (Asif Nawaz) and A.N. (Ammar Natsheh); data curation, T.H.N.; writing-original draft preparation, T.H.N.; writing-review and editing, T.L.V., A.N. (Asif Nawaz) and A.N. (Ammar Natsheh); project administration, T.L.V.; funding acquisition, T.L.V. and T.H.N. All authors have read and agreed to the published version of the manuscript.

**Funding:** This work was funded by Ho Chi Minh City University of Food Industry—Contract Number 144/HD-DCT dated 31 December 2019.

**Informed Consent Statement:** Not applicable.

**Data Availability Statement:** Not applicable.

**Conflicts of Interest:** The authors declare no conflict of interest.

## References

1. Eghtedarpour, N.; Farjah, E. Power control and management in hybrid AC/DC microgrid. *IEEE Trans. Smart Grid* **2014**, *5*, 1494–1505. [[CrossRef](#)]
2. Xiao, H.; An, L.; Shuai, Z.; Jin, G.; Huang, Y. An improved control method for multiple bidirectional power converters in hybrid AC/DC microgrid. *IEEE Trans. Smart Grid* **2016**, *7*, 340–347. [[CrossRef](#)]
3. Khan, O.; Acharya, S.; Al Hosani, M.; El Moursi, M.S. Hill climbing power flow algorithm for hybrid DC/AC microgrid. *IEEE Trans. Power Electron.* **2018**, *33*, 5532–5537. [[CrossRef](#)]
4. Sun, X.; Liu, B.; Cai, Y.; Zhang, H.; Zhu, Y.; Wang, B. Frequency-based power management for photovoltaic/battery/fuel cell-electrolyser stand-alone microgrid. *IET Power Electron.* **2016**, *9*, 2602–2610. [[CrossRef](#)]
5. Li, J.; Cai, H.; Yang, P.; Wei, W. A Bus-Sectionalized Hybrid AC/DC Microgrid: Concept, Control Paradigm, and Implementation. *Energies* **2021**, *14*, 3508. [[CrossRef](#)]
6. Xia, Y.; Wei, W.; Yu, M.; Wang, X.; Peng, Y. Power management for a hybrid AC/DC microgrid with multiple subgrids. *IEEE Trans. Power Electron.* **2018**, *33*, 3520–3533. [[CrossRef](#)]
7. Nejabatkhah, F.; Li, Y.W. Overview of power management strategies of hybrid AC/DC microgrid. *IEEE Trans. on Power Electron.* **2015**, *30*, 7072–7089. [[CrossRef](#)]
8. Ali, S.; Zheng, Z.; Aillerie, M.; Sawicki, J.-P.; Péra, M.-C.; Hissel, D. A Review of DC Microgrid Energy Management Systems Dedicated to Residential Applications. *Energies* **2021**, *14*, 4308. [[CrossRef](#)]
9. Mahmood, H.; Michaelson, D.; Jiang, J. Decentralized power management of a PV/battery hybrid unit in a droop-controlled islanded microgrid. *IEEE Trans. Power Electron.* **2015**, *30*, 7215–7229. [[CrossRef](#)]
10. Park, J.-M.; Byun, H.-J.; Kim, S.-H.; Kim, S.-H.; Won, C.-Y. DC Solid-State Circuit Breakers with Two-Winding Coupled Inductor for DC Microgrid. *Energies* **2021**, *14*, 4129. [[CrossRef](#)]
11. Guo, Z.; Sha, D.; Liao, X. Voltage magnitude and frequency control of three-phase voltage source inverter for seamless transfer. *IET Power Electron.* **2014**, *7*, 200–208. [[CrossRef](#)]
12. Babqi, A.J.; Etemadi, A.H. MPC-based microgrid control with supplementary fault current limitation and smooth transition mechanisms. *IET Gener. Transm. Distrib.* **2017**, *11*, 2164–2172. [[CrossRef](#)]

13. Mohamed, Y.A.R.I.; Zeineldin, H.H.; Salama, M.M.A.; Seethapathy, R. Seamless formation and robust control of distributed generation microgrids via direct voltage control and optimized dynamic power sharing. *IEEE Trans. Power Electron.* **2011**, *27*, 1283–1294. [[CrossRef](#)]
14. Nguyen, T.H.; Al Hosani, K.; Al Sayari, N.; Beig, A.R. Seamless transition scheme between grid-tied and stand-alone modes of distributed generation inverters. In *Proceeding of the IEEE IFEEC 2017, Kaohsiung, Taiwan, 3–7 June 2017*; pp. 344–349.
15. Liu, Z.; Liu, J.; Zhao, Y. A unified control strategy for three-phase inverter in distributed generation. *IEEE Trans. Power Electron.* **2013**, *29*, 1176–1191.
16. Balaguer, I.J.; Lei, Q.; Yang, S.; Supatti, U.; Peng, F.Z. Control for grid-connected and intentional islanding operations of distributed power generation. *IEEE Trans. Ind. Electron.* **2011**, *58*, 147–157. [[CrossRef](#)]
17. Vandoorn, T.L.; Meersman, B.; De Kooning, J.D.M.; Vandeveld, L. Transition from islanded to grid-connected mode of microgrids with voltage-based droop control. *IEEE Trans. Power Syst.* **2013**, *28*, 2545–2553. [[CrossRef](#)]
18. Tang, F.; Guerrero, J.M.; Vasquez, J.C.; Wu, D.; Meng, L. Distributed active synchronization strategy for microgrid seamless reconnection to the grid under unbalance and harmonic distortion. *IEEE Trans. Smart Grid* **2015**, *6*, 2757–2768. [[CrossRef](#)]
19. Hwang, T.S.; Park, S.Y. A seamless control strategy of a distributed generation inverter for the critical load safety under strict grid disturbances. *IEEE Trans. Power Electron.* **2018**, *28*, 4780–4790. [[CrossRef](#)]
20. Yang, S.; Wang, P.; Tang, Y. Feedback linearization-based current control strategy for modular-multilevel converters. *IEEE Trans. Power Electron.* **2018**, *33*, 161–174. [[CrossRef](#)]
21. Khazaei, J.; Tu, Z.; Asrari, A.; Liu, W. Feedback linearization control of converters with LCL filter for weak AC grid integration. *IEEE Trans. Power Syst.* **2021**, *36*, 3740–3750. [[CrossRef](#)]
22. Lou, G.; Gu, W.; Wang, J.; Wang, J.; Gu, B. A unified control scheme based on a disturbance observer for seamless transition operation of inverter-interfaced distributed generation. *IEEE Trans. Smart Grid* **2018**, *9*, 5444–5454. [[CrossRef](#)]
23. Chen, C.L.; Wang, Y.; Lai, J.S.; Lee, Y.S.; Martin, D. Design of parallel inverters for smooth mode transfer microgrid applications. *IEEE Trans. Power Electron.* **2009**, *25*, 6–15. [[CrossRef](#)]
24. Kim, K.H.; Jeung, Y.C.; Lee, D.C.; Kim, H.G. LVRT scheme of PMSG wind power system based on feedback linearization. *IEEE Trans. Power Electron.* **2012**, *27*, 2376–2384. [[CrossRef](#)]
25. Ostadijafari, M.; Dubey, A.; Yu, N. Linearized price-responsive HVAC controller for optimal scheduling of smart building loads. *IEEE Trans. Smart Grid* **2020**, *11*, 3131–3145. [[CrossRef](#)]
26. Slotine, J.J.E.; Li, W. *Applied Nonlinear Control*; Prentice-Hall: Englewood Cliffs, NJ, USA, 1991; pp. 207–271.
27. Kim, D.-E.; Lee, D.-C. Feedback linearization control of three-phase UPS inverter system. *IEEE Trans. Ind. Electron.* **2010**, *57*, 963–968.
28. Jeong, S.-Y.; Nguyen, T.H.; Le, Q.A.; Lee, D.-C. High-performance control of three-phase four-wire DVR systems using feedback linearization. *J. Power Electron.* **2016**, *16*, 351–361. [[CrossRef](#)]
29. Al Hosani, K.; Nguyen, T.H.; and Al Sayari, N. An improved control strategy of 3P4W DVR systems under unbalanced and distorted voltage conditions. *Int. J. Electr. Power Energy Syst.* **2018**, *98*, 233–242. [[CrossRef](#)]
30. Nguyen, T.H.; Lee, D.C. Advanced fault ride-through technique for PMSG wind turbine systems using line-side converter as STATCOM. *IEEE Trans. Ind. Electron.* **2013**, *60*, 2842–2850. [[CrossRef](#)]